PHYSICAL REVIEW D **88,** 063516 (2013)

Milli-interacting dark matter

Quentin Wallemacq*

IFPA, Département AGO, Université de Liège, Sart Tilman, 4000 Liège, Belgium

(Received 30 July 2013; published 12 September 2013)

We present a dark matter model reproducing well the results from DAMA/LIBRA and CoGeNT and having no contradiction with the negative results from XENON100 and CDMS-II/Ge. Two new species of fermions F and G form hydrogenlike atoms with standard atomic size through a dark $U(1)$ gauge interaction carried out by a dark massless photon. A Yukawa coupling between the nuclei F and neutral scalar particles S induces an attractive shorter-range interaction. This dark sector interacts with our standard particles because of the presence of two mixings, a kinetic photon–dark photon mixing, and a mass σ-S mixing. The dark atoms from the halo diffuse elastically in terrestrial matter until they thermalize and then reach underground detectors with thermal energies, where they form bound states with nuclei by radiative capture. This causes the emission of photons that produce the signals observed by direct-search experiments.

DOI: 10.1103/PhysRevD.88.063516 PACS numbers: 95.35.+d

I. INTRODUCTION

Direct searches for dark matter have been accumulating results in recent years, starting with the DAMA/NaI experiment that observed a significant signal since the late 1990s. Its successor, DAMA/LIBRA, has further confirmed the signal and improved its statistical significance to a current value of 8.9σ [1]. Some other experiments such as CoGeNT [2], CRESST-II [3], and very recently CDMS-II/Si [4] are going in the same direction and report observations of events in their underground detectors, while others, such as XENON100 [5] or CDMS-II/Ge [6] continue to rule out any detection. These experiments challenge the usual interpretation of dark matter as being made only of weakly interacting massive particles (WIMPs). Because of the motion of the Solar System in the galactic dark-matter halo, incident WIMPs would hit underground detectors where they could produce nuclear recoils, which would then be the source of the observed signals. However, this interpretation of the data induces strong contradictions between experiments with positive and negative results as well as tensions between experiments with positive results [5].

In this context, alternatives have been proposed to reconcile the experiments. Among them, mirror matter [7] and millicharged atomic dark matter [8] provide explanations respectively in terms of Coulomb scattering of millicharged mirror nuclei on nuclei in the detectors or in terms of hyperfine transitions of millicharged dark atoms analogous to hydrogen colliding on nuclei. In these scenarios, millicharged dark species are obtained by a kinetic mixing between standard photons and photons from the dark sector. Mirror matter in the presence of kinetic photon–mirror photon mixing gives a rich phenomenology that can reproduce the signals of most of the experiments, but some tensions remain with experiments such as XENON100 or EDELWEISS. Millicharged atomic dark matter can explain the excess of events reported by CoGeNT but keeps the contradictions with the others.

Another scenario has been proposed by Khlopov *et al.* [9,10], in which new negatively charged particles (O^{--}) are bound to primordial helium (He^{++}) in neutral O-helium dark atoms (OHe). The approach here is quite different because the interactions of these OHe with terrestrial matter are determined by the nuclear interactions of the helium component. Therefore, instead of producing nuclear recoils, these dark atoms would thermalize in the Earth by elastic collisions and reach underground detectors with thermal energies, where they form bound states with nuclei by radiative capture, the emitted photon being the source of the signal. Therefore, the observation of a signal depends on the existence of a bound state in the OHe-nucleus system and can provide a natural explanation to the negative results experiments, in case of the absence of bound states with the constituent nuclei. However, a careful analysis of the interactions of OHe atoms with nuclei [11] has ruled out the model. Nevertheless, the scenario presented here keeps many of the features of the OHe, but avoids its problems.

Our model aims at solving the discrepancies between experiments with positive results, as well as to reconcile them with those without any signal. It presents common features with the ones mentioned above [7–9]. It contains dark fermions that possess electric millicharges due to the same kind of photon–dark photon mixing as in the mirror and atomic-dark-matter scenarios, but also another mixing between σ mesons and new dark-scalar particles creating an attractive interaction with nucleons, which couple to σ mesons in the framework of an effective Yukawa theory. The dark matter will be in the form of hydrogenoid atoms with standard atomic sizes that interact sufficiently with terrestrial matter to thermalize before reaching underground

*quentin.wallemacq@ulg.ac.be

detectors. There, dark and standard nuclei will form bound states by radiative capture through the attractive exchange between dark fermions and nuclei.

An important feature of such a model is that it presents a self-interacting dark matter, on which constraints exist from the Bullet cluster or from halo shapes [12]. According to [13], these can be avoided if the self-interacting candidate is reduced to at most 5% of the dark matter mass content of the galaxy, the rest being constituted by conventional collisionless particles. In the following, the dark sector will therefore be a subdominant part of dark matter.

In Sec. II, the ingredients and the effective Lagrangian of the model are described. Constraints from vector-meson disintegrations are considered and the interaction potentials between dark and standard sectors are derived in Sec. III, from the Lagrangian of Sec. II. The thermalization of the dark atoms in terrestrial matter is studied in Sec. IV and constraints on model parameters are obtained, to thermalize between the surface and an underground detector. The radiative-capture process within a detector is described in Sec. V, where the capture cross section and the event rate are derived. Section VI gives an overview of the reproduction of the experimental results.

II. THE MODEL

We postulate that a dark, hidden, sector exists, consisting of two kinds of new fermions, denoted by F and G, respectively coupled to dark photons Γ with opposite couplings $+e'$ and $-e'$, while only F is coupled to neutral dark scalars S with a positive coupling g'. This dark sector is governed by the Lagrangian

$$\mathcal{L}^{\text{dark}} = \mathcal{L}_0^{\text{dark}} + \mathcal{L}_{\text{int}}^{\text{dark}}, \tag{1}$$

where the free and interaction Lagrangians $\mathcal{L}_0^{\text{dark}}$ and $\mathcal{L}_{\text{int}}^{\text{dark}}$ have the forms

$$\mathcal{L}_0^{\text{dark}} = \sum_{k=F,G} \bar{\psi}_k (i\gamma^\mu \partial_\mu - m_k)\psi_k - \frac{1}{4} F'^{\mu\nu} F'_{\mu\nu} + \frac{1}{2}\partial_\mu \phi_S \partial^\mu \phi_S - \frac{1}{2} m_S \phi_S^2 \tag{2}$$

and

$$\mathcal{L}_{\text{int}}^{\text{dark}} = e' \bar{\psi}_F \gamma^\mu A'_\mu \psi_F - e' \bar{\psi}_G \gamma^\mu A'_\mu \psi_G + g' \phi_S \bar{\psi}_F \psi_F. \tag{3}$$

Here, $\psi_{F(G)}$, A', and ϕ_S are respectively the fermionic, vectorial, and real scalar fields of the dark fermion $F(G)$, dark photon Γ and dark scalar S, while $m_{F(G)}$ and m_S are the masses of the $F(G)$ and S particles. F' stands for the electromagnetic-field-strength tensor of the massless dark photon Γ.

Moreover, we assume that the dark photons Γ and the dark scalars S are mixed respectively with the standard photons γ and neutral mesons σ through the mixing Lagrangian,

$$\mathcal{L}_{\text{mix}} = \frac{1}{2}\tilde{\epsilon} F^{\mu\nu} F'_{\mu\nu} + \tilde{\eta}(m_\sigma^2 + m_S^2)\phi_\sigma \phi_S, \tag{4}$$

where $m_\sigma = 600$ MeV [14] is the mass of σ and $\tilde{\epsilon}$ and $\tilde{\eta}$ are the dimensionless parameters of kinetic γ-Γ and mass σ-S mixings. These are supposed to be small compared with unity.

The model therefore contains seven free parameters, m_F, m_G, m_S, e', g', $\tilde{\epsilon}$ and $\tilde{\eta}$, and the total Lagrangian of the combined standard and dark sectors is

$$\mathcal{L} = \mathcal{L}^{\text{SM}} + \mathcal{L}^{\text{dark}} + \mathcal{L}_{\text{mix}}, \tag{5}$$

where $\mathcal{L}^{\text{SM}}$ stands for the Lagrangian of the standard model.

The F and G fermions will form dark hydrogenoid atoms in which F will play the role of a dark nucleus binding to nuclei in underground detectors, while G acts as a dark electron. F has then to be heavy enough to form bound states and we will seek masses of F between 10 GeV and 10 TeV, while requiring $m_G \ll m_F$. Due to the mass mixing term in (4), F will interact with nucleons through the exchange of S and this attractive interaction will be responsible for the binding. It cannot be too long ranged but it must allow the existence of nucleus–F bound states of at least the size of the nucleus. Because the range of the interaction is of the order of m_S^{-1}, this leads us to consider values of the mass of S between 100 keV and 10 MeV. The other four parameters will not be directly constrained by the direct-search experiments, but only the products $\tilde{\epsilon}e'$ and $\tilde{\eta}g'$. However, a reasonable choice seems to be $\tilde{\epsilon}, \tilde{\eta} \ll 1$ together with $e' \simeq e$ and $g' \simeq g$, where e is the charge of the proton and $g = 14.4$ [15] is the Yukawa coupling of the nucleon to the σ meson. In summary, we will consider:

$$10\ \text{GeV} \leq m_F \leq 10\ \text{TeV}, \qquad 100\ \text{keV} \leq m_S \leq 10\ \text{MeV},$$
$$m_G \ll m_F, \qquad e' \simeq e, \qquad g' \simeq g, \qquad \tilde{\epsilon}, \tilde{\eta} \ll 1.$$

III. DARK-STANDARD INTERACTIONS

The mixings described by (4) induce interactions [7,8] between dark fermions F and G and our standard particles. It is well known that, to first order in $\tilde{\epsilon}$, a kinetic mixing such as the one present in (4) will make the dark particles F and G acquire small effective couplings $\pm\tilde{\epsilon}e'$ to the standard photons. One can define the kinetic mixing parameter in terms of the electric charge of the proton e through $\epsilon e \equiv \tilde{\epsilon}e'$, which means that the particles F and G will interact electromagnetically with any charged particle of the standard model with millicharges $\pm\epsilon e$.

The mass mixing from (4) characterized by $\tilde{\eta}$ induces an interaction between F and σ, through the exchange of S, and hence an interaction between F and any standard particle coupled to σ, e.g. the proton and the neutron in

the framework of an effective Yukawa theory. Since $\tilde{\eta}$ is small, the interaction is dominated by one $\sigma + S$ exchange and the amplitude of the process has to be determined before passing to the nonrelativistic limit in order to obtain the corresponding interaction potential. As for ϵ introduced above, one defines η by $\eta g = \tilde{\eta} g'$. In the following, except in Sec. III A, ϵ and η will be used instead of $\tilde{\epsilon}$ and $\tilde{\eta}$.

In a similar way as in [8], the dark fermions F and G will bind to form neutral dark hydrogenoid atoms of Bohr radius $a'_0 = \frac{1}{\mu\alpha'}$, where μ is the reduced mass of the $F - G$ system and $\alpha' = \frac{e'}{4\pi}$. In principle, the galactic dark matter halo could be populated by these neutral dark atoms as well as by a fraction of dark ions F and G, but Ref. [16] shows that supernovae shock waves will evacuate millicharged dark ions from the disk and that galactic magnetic fields will prevent them from reentering unless $\epsilon < 9 \times 10^{-12}\,(m_{F,G}/\mathrm{GeV})$, which is far below the values that we will be interested in the following to explain the signals of the direct-dark-matter-search experiments. Therefore, the signals will only be induced by the interactions of the dark atoms with matter in the detectors.

A. Constraints from Υ and J/ψ disintegrations

A direct consequence of the mass mixing term in (4) is that a certain fraction of σ's can convert into S scalars and then evade in the dark sector. This can be seen in the disintegrations of quarkonium states such as the J/ψ meson and the $1S$ and $3S$ resonances of the Υ meson. The studied and unseen processes are generically represented by

$$Q\bar{Q} \to \sigma\bar{\sigma} \to S\bar{S}, \qquad Q\bar{Q} \to \gamma\sigma \to \gamma S, \tag{6}$$

where $Q\bar{Q} = \Upsilon(1S)$, $\Upsilon(3S)$ or $J/\psi(1S)$. Because of the parity -1 of these states, the disintegration in two particles of parity $+1$ is forbidden, and one hence avoids the constraints from the first process. From [17–19], the 90% C.L. upper limits on the branching ratios of the second process are respectively

$$\begin{aligned} B(\Upsilon(1S) \to \gamma S) &< 5.6 \times 10^{-5}, \\ B(\Upsilon(3S) \to \gamma S) &< 15.9 \times 10^{-6}, \\ B(J/\psi(1S) \to \gamma S) &< 4.3 \times 10^{-6}. \end{aligned} \tag{7}$$

In the limit where the momenta of the constituent quarks are null [$p = (M_{Q\bar{Q}}/2, \vec{0})$, where $M_{Q\bar{Q}}$ is the mass of the $Q\bar{Q}$ meson], we get

$$\begin{aligned} &\frac{B(Q\bar{Q} \to \gamma S)}{B(Q\bar{Q} \to e^+e^-)} \\ &= \frac{2\beta}{\alpha} \frac{M_{Q\bar{Q}}(M_{Q\bar{Q}}^2 - m_S^2)}{(M_{Q\bar{Q}}^2 + 2m_e^2)\sqrt{M_{Q\bar{Q}}^2 - 4m_e^2}} \frac{\tilde{\eta}^2(m_\sigma^2 + m_S^2)^2}{(m_S^2 - m_\sigma^2)^2}, \end{aligned} \tag{8}$$

where $B(Q\bar{Q} \to e^+e^-)$ is the branching ratio of the disintegration of $Q\bar{Q}$ into a positron-electron pair, $\alpha = \frac{e^2}{4\pi} = \frac{1}{137}$ is the fine structure constant, $\beta = \frac{g^2}{4\pi} = 16.5$, and m_e is the mass of the electron. $B(Q\bar{Q} \to e^+e^-) = (2.38 \pm 0.11)\%$, $(2.03 \pm 0.20)\%$ and $(5.94 \pm 0.06)\%$ [14], respectively for $Q\bar{Q} = \Upsilon(1S)$, $\Upsilon(3S)$ and $J/\psi(1S)$.

Putting together (7) and (8), one gets allowed regions for parameters $\tilde{\eta}$ and m_S from processes (7). But for the rather small values of m_S considered here, expression (8) turns out to be independent of the mass of the scalar particle and the most stringent constraint comes from the disintegration of $J/\psi(1S)$:

$$\tilde{\eta} < 1.2 \times 10^{-4}. \tag{9}$$

B. Interactions of F and G fermions with nucleons and electrons

The kinetic and mass mixings introduced in the Lagrangian of the model give rise, in the nonrelativistic limit, to interaction potentials between the particles F and G and standard protons, neutrons and electrons.

The kinetic $\gamma - \Gamma$ mixing induces a Coulomb interaction with protons or electrons with a potential given by

$$V_C(r) = \pm \frac{\epsilon\alpha}{r}, \tag{10}$$

where the plus sign is for the proton-F and electron-G couplings, and the minus sign for the electron-F and proton-G interactions.

The $\sigma - S$ mass mixing gives rise, in the nonrelativistic limit, to the one $\sigma + S$-exchange potential between F and a nucleon

$$V_M(r) = -\frac{\eta(m_\sigma^2 + m_S^2)\beta}{r}\left(\frac{e^{-m_\sigma r} - e^{-m_S r}}{m_S^2 - m_\sigma^2}\right). \tag{11}$$

Note that in the limit $m_S \to m_\sigma$, expression (11) becomes $V_M(r) = -\frac{\eta m_\sigma \beta}{2} e^{-m_\sigma r}$, although this particular case will not be considered in the following.

IV. THERMALIZATION OF DARK FG ATOMS IN TERRESTRIAL MATTER

Because of the motion of the Earth (and of the Sun) through the Galactic dark matter halo, an effective wind of dark atoms hits the surface of our planet. These dark atoms penetrate the surface and undergo elastic collisions with terrestrial atoms, and lose part of their energy at each collision. If the number of collisions and the elastic-diffusion cross section are sufficiently large, then the dark atoms can deposit all their energy in the terrestrial matter before going out on the other side of the Earth, or even thermalize between the surface and an underground detector. The diffusions can be of two types: electromagnetic (atom-dark atom) and $\sigma + S$-exchange (nucleus-F), from potentials (10) and (11). In the following, we shall consider the terrestrial surface as made of "average"

atoms of silicon, with atomic and mass numbers $Z_m = 14$ and $A_m = 28$ and mass $m_m = A_m m_p$, where m_p is the mass of the proton. The nuclear radius will be neglected here, since it is much smaller than the wavelength of the incident particles at these energies, and has therefore no influence on the elastic cross section.

A. Interaction of dark *FG* atoms with terrestrial atoms

We assume that $m_F \gg m_G$, and hence that $m_{FG} \simeq m_F$, where m_{FG} is the mass of an FG dark atom, so that in the dark bound state FG, F plays the role of a dark nucleus while G is spherically distributed around it. In this context, the dark FG atoms, as well as the terrestrial ones, are assimilated to uniformly charged spheres of charges $-\epsilon e$ and $-Z_m e$ and radii a_0' and a_0, representing the respective electronic clouds, with opposite pointlike charges at their centers, corresponding to the respective F and silicon nuclei. Because the elastic interaction cross section of a dark atom with a terrestrial atom has to be large enough to allow thermalization before reaching an underground detector, the atomic size of a dark atom will be of the same order as a standard one. We take 1 Å as a reference for the atomic size and set $a_0' = \frac{1}{m_G \alpha'} = a_0 = 1$ Å. In view of the suggestion $e' \simeq e$ of Sec. II, this gives $m_G \simeq m_e$.

We then obtain the atom–dark atom electrostatic interaction potential as:

$$\begin{aligned} V_{\rm at} &= \frac{\epsilon Z_m \alpha}{160 a_0^6}\left(-r^5 + 30 a_0^2 r^3 + 80 a_0^3 r^2 - 288 a_0^5 + \frac{160 a_0^6}{r}\right), \qquad r < a_0 \\ &= \frac{\epsilon Z_m \alpha}{160 a_0^6}\left(-r^5 + 30 a_0^2 r^3 - 80 a_0^3 r^2 + 192 a_0^5 - \frac{160 a_0^6}{r}\right), \qquad a_0 < r < 2a_0 \\ &= 0, \qquad r > 2a_0 \end{aligned} \tag{12}$$

r being the distance between both nuclei and "at" standing for "*atomic*."

The shape of $V_{\rm at}$ is represented in Fig. 1 for a silicon atom and for the best fit value of the kinetic mixing parameter $\epsilon = 6.7 \times 10^{-5}$, discussed in Sec. VI. It shows a very shallow potential well at $r \simeq a_0$. Its depth, of the order of 10^{-3} eV, does not allow to create atom–dark atom bound states, as they would be destroyed by thermal excitation in the Earth, where $T \sim 300$ K corresponds to thermal energies of the order of 10^{-2} eV. At smaller distance, when $r \lesssim 0.6$ Å, the Coulomb repulsion between nuclei starts to dominate. Thus, no atomic bound state can form with elements between the surface and an underground detector.

In addition to this atom–dark atom interaction, both nuclei interact through $\sigma + S$ exchange, corresponding to the potential (11) multiplied by the number of nucleons in a silicon nucleus:

$$V_{\rm nucl}(r) = -\frac{\eta(m_\sigma^2 + m_S^2) A_m \beta}{r}\left(\frac{e^{-m_\sigma r} - e^{-m_S r}}{m_S^2 - m_\sigma^2}\right), \tag{13}$$

where "nucl" stands for "*nuclear*." Because $m_\sigma \gg m_S$, this potential is very similar to a pure Yukawa potential $\sim -\frac{1}{r} e^{-mr}$. Although it creates a deeper attractive well at short distance (of the order of $m_S^{-1} \simeq 100$ fm), this narrower potential will neither admit stable bound states with the relatively light nuclei present in terrestrial matter. Therefore, the interactions of FG dark atoms in the Earth can be considered as purely elastic.

B. Elastic diffusion cross section

The elastic differential cross sections corresponding to the potentials (12) and (13) can be obtained by evaluating the square of the modulus of the diffusion amplitude in the framework of the Born approximation in the center-of-mass frame of the nucleus-F system:

$$\left(\frac{d\sigma}{d\Omega}\right)_{\rm at} = \frac{\mu^2 \epsilon^2 Z_m^2 \alpha^2}{a_0^{12}} \frac{1}{K^{16}} I^2 \tag{14}$$

with

$$\begin{aligned} I = {} & 9(K^2 a_0^2 + 1) + 9\cos(2Ka_0)(K^2 a_0^2 - 1) \\ & + 12\cos(Ka_0) K^4 a_0^4 - 18\sin(2Ka_0) Ka_0 \\ & - 12\sin(Ka_0) K^3 a_0^3 + 2K^6 a_0^6 \end{aligned}$$

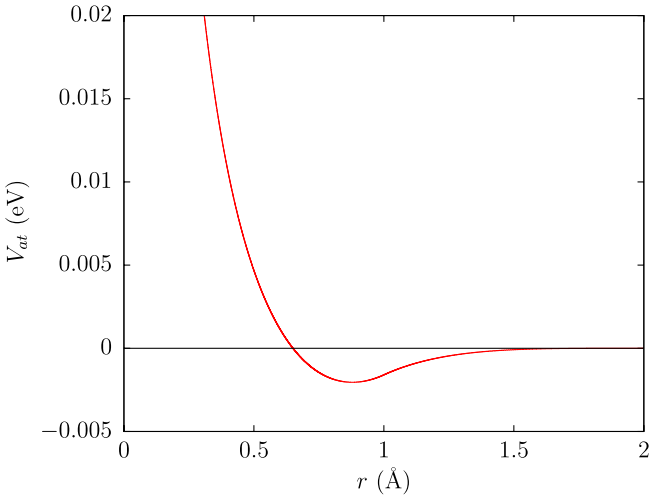

FIG. 1 (color online). Shape of the silicon-FG interaction potential $V_{\rm at}$ (eV) as a function of the distance between nuclei r (Å), with the best fit value $\epsilon = 6.7 \times 10^{-5}$.

and

$$\left(\frac{d\sigma}{d\Omega}\right)_{\rm nucl} = 4\mu^2\eta^2 A_m^2\beta^2\left(\frac{m_\sigma^2+m_S^2}{m_S^2-m_\sigma^2}\right)^2 \times\left[\frac{1}{m_\sigma^2+K^2}-\frac{1}{m_S^2+K^2}\right]^2, \quad (15)$$

where $K = 2k\sin\theta/2$ and $k = \sqrt{2\mu E}$ are the transferred and initial momenta. θ is the deflection angle with respect to the collisional axis and $\mu = \frac{m_F m_m}{m_F+m_m}$ is the reduced mass of the nucleus-F system.

The total differential cross section corresponding to $V_{\rm at}+V_{\rm nucl}$ is finally given by the sum of (14) and (15) without forgetting the interference term:

$$\left(\frac{d\sigma}{d\Omega}\right)_{\rm tot} = \left(\frac{d\sigma}{d\Omega}\right)_{\rm at} + \left(\frac{d\sigma}{d\Omega}\right)_{\rm nucl} - \frac{4\mu^2\epsilon\eta Z_m A_m\alpha\beta}{a_0^6} \times\left(\frac{m_\sigma^2+m_S^2}{m_S^2-m_\sigma^2}\right)\frac{I}{K^8}\left[\frac{1}{m_\sigma^2+K^2}-\frac{1}{m_S^2+K^2}\right]. \quad (16)$$

C. Energy loss per unit path length: $\frac{dE}{dx}$

At each collision with an atom at rest in the terrestrial surface, a dark atom loses an energy $\triangle K = \frac{p^2(\cos\theta-1)}{m_m}$ in the frame of the Earth, where p is the momentum of each atom in the center-of-mass frame. The energy loss per unit length in the frame of the Earth is then obtained by integrating over all diffusion angles,

$$\frac{dE}{dx} = n_m\int_\Omega \triangle K\left(\frac{d\sigma}{d\Omega}\right)_{\rm tot} d\Omega, \quad (17)$$

where n_m is the number density of terrestrial atoms.

Of course, the linear path approximation is valid only when $m_F \gg m_m$, but it gives in the other cases an upper limit on the penetration length of the dark atoms through the Earth, which is of interest here. To obtain it, one just needs to integrate the inverse of (17) from the initial energy of the dark atoms E_0 to the thermal energy of the medium $E_{th} = \frac{3}{2}T_m$, where T_m is the temperature

$$x = \int_{E_{th}}^{E_0}\frac{dE}{|dE/dx|}. \quad (18)$$

D. Penetration at a depth of 1 km

Figure 2 shows the region (in blue) of mixing parameters ϵ and η where $x \leq 1$ km, 1 km being the typical depth at which underground detectors are located, for the best fit values $m_F = 650$ GeV and $m_S = 0.426$ MeV obtained in Sec. VI. In the blue region, thermalization occurs before reaching 1 km, while outside the dark atoms hit the detector with nonthermal energies and can cause nuclear recoils. The best-fit model, characterized by $m_F = 650$ GeV, $m_S = 0.426$ MeV, $\epsilon = 6.7\times10^{-5}$ and $\eta = 2.2\times10^{-7}$ clearly satisfies the condition with $x \simeq 40$ m.

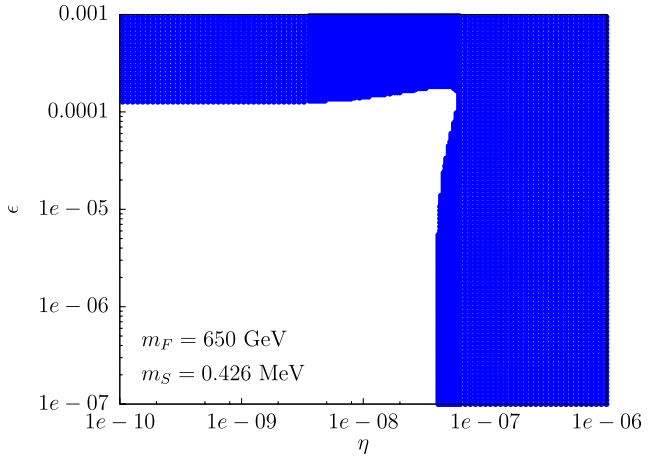

FIG. 2 (color online). Region of parameters ϵ and η (blue) where thermalization of dark atoms occurs before reaching 1 km underground, for the best fit parameters $m_F = 650$ GeV and $m_S = 0.426$ MeV obtained in Sec. VI.

Some interesting features are present in Fig. 2. At low η ($\eta \lesssim 10^{-9}$), thermalization is realized entirely by the electromagnetic atom–dark atom interaction $V_{\rm at}$, for sufficiently large ϵ ($\epsilon \gtrsim 10^{-4}$). When η increases ($10^{-9} \lesssim \eta \lesssim 3\times10^{-8}$), the limit on ϵ slightly increases. This counterintuitive behavior is due to the negative interference term present in the total elastic cross section (16) that increases with η. For a certain range of η ($3\times10^{-8} \lesssim \eta \lesssim 6\times10^{-8}$), three regimes are visible: the first at low ϵ, where thermalization is mostly ensured by the nuclear interaction; the second at intermediate ϵ, where thermalization before 1 km is not possible because the interference term partly compensates $(\frac{d\sigma}{d\Omega})_{\rm at}$ and $(\frac{d\sigma}{d\Omega})_{\rm nucl}$ in (16); the third at higher ϵ, where thermalization is dominated by $V_{\rm at}$. Finally, at higher η ($\eta \gtrsim 6\times10^{-8}$), all values of ϵ are possible, meaning that nuclear interaction alone would be sufficient to thermalize.

V. INTERACTIONS IN UNDERGROUND DETECTORS

The dark atoms thermalize by elastic collisions in terrestrial matter between the surface and the underground detector. Once they reach thermal energies, they start drifting towards the center of the earth until they reach the detector, where they undergo collisions with the atoms of the active medium. Because of the Coulomb barrier due to the repulsion between nuclei (seen in Fig. 1 at $r \lesssim 0.6$ Å), most of these collisions are elastic but sometimes tunneling through the barrier can occur and bring a dark nucleus F into the region of the potential well present at smaller distance, due to the exchange of σ and S between F and the nuclei of the detector. There, E1 transitions produce deexcitation of the system to low-energy bound

states by emission of photons that can be detected, causing the observed signal. In the following, only the part of the potential that is relevant for the capture process is considered, i.e. the region $0 < r \lesssim 0.6$ Å, where the interaction is dominated by the exchanges between F and the nucleus. The long-range part of the potential, 10^3 to 10^4 times smaller, does not affect the initial diffusion eigenstate and the final bound state of the process and is therefore neglected, and the dilute electronic and G distributions, mostly transparent to each other, follow passively their respective nuclei.

A. Interactions of fermions F with nuclei

Because of their interactions with nucleons, the dark particles F interact with nuclei. If a nucleus N of mass number A and atomic number Z is seen as a uniformly charged sphere of radius $R = r_0 A^{1/3}$, the integration of expressions (10) and (11) over its electric and nuclear charge distributions gives

$$V_C^N(r) = \frac{\epsilon Z\alpha}{2R}\left(3 - \frac{r^2}{R^2}\right), \qquad r < R$$
$$= \frac{\epsilon Z\alpha}{r}, \qquad r > R \tag{19}$$

for the Coulomb potential, and

$$\begin{aligned} V_M^N(r<R) = &-\frac{V_0}{r}[2r(m_\sigma^{-2} - m_S^{-2}) \\ &+ (R + m_\sigma^{-1})m_\pi^{-2}(e^{-m_\sigma r} - e^{m_\sigma r})e^{-m_\sigma R} \\ &- (R + m_S^{-1})m_S^{-2}(e^{-m_S r} - e^{m_S r})e^{-m_S R}], \\ V_M^N(r>R) = &-\frac{V_0}{r}[m_\sigma^{-2}e^{-m_\sigma r}(e^{m_\sigma R}(R - m_\sigma^{-1}) \\ &+ e^{-m_\sigma R}(R + m_\sigma^{-1})) \\ &- m_S^{-2}e^{-m_S r}(e^{m_S R}(R - m_S^{-1}) \\ &+ e^{-m_S R}(R + m_S^{-1}))] \end{aligned} \tag{20}$$

for the one $\sigma + S$-exchange potential between F and a nucleus. In expression (20), $V_0 = 3\eta(m_\sigma^2 + m_S^2)\beta/(2r_0^3(m_S^2 - m_\sigma^2))$, where $r_0 = 1.2$ fm.

Figure 3 shows the shape of the total potential $V^N = V_C^N + V_M^N$ for light, intermediate and heavy nuclei, all involved in underground detectors: sodium (DAMA/LIBRA), germanium (CoGeNT, CDMS-II), iodine (DAMA/LIBRA), and xenon (XENON100). All these potentials exhibit a Coulomb barrier, then an attractive well at shorter distance. The height of the barrier as well as the depth and the width of the well are determined by the values of the parameters ϵ, η and m_S, taken here equal to the preferred values of Sec. VI, but also depend on the nucleus. Typically, the depth of the well is of several keV and the Coulomb barrier goes up to several eV with a maximum being localized at about 2000 fm.

B. Bound-state-formation mechanism

At thermal energies, to order v/c, only the partial s wave of an incident plane wave on an attractive center is affected by the potential. Considering the center-of-mass frame of the nucleus-F system, this means that the largest contribution to tunneling corresponds to tunneling through the Coulomb barrier at zero relative angular momentum l. Due to selection rules, electric dipole transitions E1 to final bound states at $l = 0$ are forbidden. It can also be shown that magnetic dipole and electric quadrupole transitions M1 and E2 to such final levels are not present [20], leaving only the possibility of captures of the particles F in two steps, i.e. first to levels at $l = 1$ after tunneling and then to levels at $l = 0$, each one corresponding to an E1 transition. The radiative capture of thermal particles F therefore requires the existence of bound states at least up to $l = 1$ in the potential wells of Fig. 3.

The transition probability per unit time for an electric multipole radiation of order q is given by [20]

$$\lambda(q, m) = \frac{8\pi(q+1)}{q[(2q+1)!!]}\omega^{2q+1}|Q_{qm}|^2, \tag{21}$$

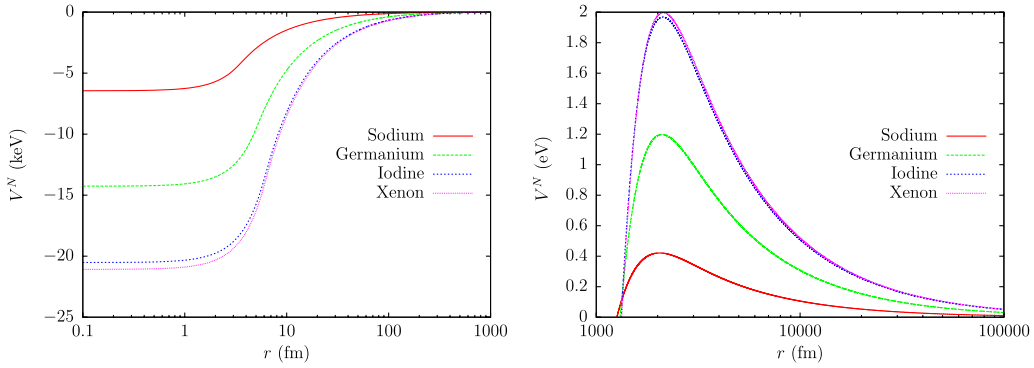

FIG. 3 (color online). Shape of the total nucleus-F interaction potential for light (solid red), intermediate (long dashed green) and heavy (short dashed blue, dotted magenta) nuclei constituting underground detectors. The attractive part (nuclear well) is on the left (keV) and the repulsive region (Coulomb barrier) is on the right (eV). The preferred parameters of Sec. VI have been used.

where $m = -q, \ldots, q$, ω is the angular frequency of the emitted radiation and the matrix element $Q_{qm} = e\sum_{j=1}^{N}\int r_j^q Y_q^{m*}(\theta_j, \varphi_j)\psi_f^*\psi_i d\vec{r}$. The sum is over all the electric charges e_j of the system and the spherical harmonics Y_q^m are evaluated at the positions of each of them. ψ_i and ψ_f are respectively the initial and final states of the transition.

In the framework of this model, one has for the E1 capture from an s state in the continuum to a bound p state, expressed in the center-of-mass frame of the nucleus-F system in terms of relative coordinates $\vec{r} = \vec{r_F} - \vec{r_N}$:

$$\lambda(1,m) = \frac{16\pi}{9}\omega^3|Q_{1m}|^2,$$
$$Q_{1m} = Ze\left(\frac{m_F}{m_F+m}\right)\int rY_1^{m*}(\theta,\varphi)\psi_f^*(\vec{r})\psi_i(\vec{r})d\vec{r}, \quad (22)$$

where m is the mass of the nucleus. The term in Q_{1m} due to the millicharged dark ion F has been neglected with respect to the term of the nucleus because of the factor ϵ, that brings a factor ϵ^2 in the transition probability. The initial and final states are expressed as

$$\psi_i(\vec{r}) = \frac{1}{k}R(r), \qquad \psi_f(\vec{r}) = R_f(r)Y_1^{-1,0,1}(\theta,\varphi), \quad (23)$$

R and R_f being respectively the radial parts of the eigenfunctions of the system at relative angular momenta $l = 0$ and $l = 1$, corresponding to energies E (positive, incident) and E_f (negative, lowest bound energy level at $l = 1$) in the center-of-mass frame. $k = \sqrt{2\mu E}$, where μ is the reduced mass of the nucleus-F system, is the momentum of the incident plane wave. The factor $\frac{1}{k}$ comes from the decomposition of a plane wave into partial waves.

The link between the transition probability $\lambda(1, m)$ and the capture cross section $\sigma_{\text{capt}}(1, m)$ is made via the relation $\lambda(1, m) = n\sigma_{\text{capt}}(1, m)v$, where n is the number density of incident particles and $v = |\vec{v}_F - \vec{v}_N|$ is the relative velocity. ψ_i is normalized in such a way that there is one incident particle per unit volume ($n = 1$), by numerically solving the radial Schrodinger equation at $l = 0$ for the positive energy E and matching the function $R(r)$ with the asymptotically free amplitude. The total E1 capture cross section σ_{capt} is then obtained by summing the cross sections corresponding to the three possible values of m and one finally gets

$$\sigma_{\text{capt}} = \frac{32\pi^2Z^2\alpha}{3\sqrt{2}}\left(\frac{m_F}{m_F+m}\right)^2\frac{1}{\sqrt{\mu}}\frac{(E-E_f)^3}{E^{3/2}}D^2, \quad (24)$$

where $D = \int_0^\infty rR_f(r)R(r)r^2dr$ and $\mu = \frac{m_F m}{m_F+m}$ is the reduced mass of the F-nucleus system. R_f and E_f are obtained by solving the radial Schrodinger equation at $l = 1$ with the WKB approximation and R_f is normalized by demanding that $\int R_f^2(r)r^2dr = 1$.

We note here that the interaction mechanism of these dark atoms in underground detectors is radically different from the standard WIMP scenario since the emitted photons produce electron recoils instead of nuclear recoils in the latter case. In experiments without any discrimination between these two kinds of recoils (DAMA/LIBRA, CoGeNT), the signals can be directly reinterpreted in terms of bound-state-formation events. On the other hand, some detectors (XENON100, CDMS-II, CRESST-II) are able to discriminate between nuclear and electron recoils. If such a detector (XENON100, CDMS-II/Ge) has negative results, then the considered dark atoms constitute good candidates because, even if bound-state-formation events cannot be suppressed naturally in the framework of the model, the remaining events will be interpreted as backgrounds and rejected. Some difficulties may appear if an experiment with a discrimination power has positive results (CDMS-II/Si, CRESST-II), since the thermalized dark atoms do not have sufficient energies to produce nuclear recoils.

C. Event counting rate

In the active medium of a detector made of nuclei N at temperature T, both F and N have velocity distributions $P_F(\vec{v_F}^{\text{lab}})$ and $P_N(\vec{v_N}^{\text{lab}})$, where "lab" stands for "laboratory frame." We take them of the same Maxwellian form

$$P_F(\vec{v_F}^{\text{lab}}) = P(\vec{v_F}^{\text{lab}}) = \left(\frac{m_F}{2\pi T}\right)^{3/2}e^{-m_F v_F^{\text{lab}2}/2T},$$
$$P_N(\vec{v_N}^{\text{lab}}) = P(\vec{v_N}^{\text{lab}}) = \left(\frac{m}{2\pi T}\right)^{3/2}e^{-m v_N^{\text{lab}2}/2T}. \quad (25)$$

The event counting rate R per unit volume of the detector is given by

$$R = n_F n_N\langle\sigma_{\text{capt}}v\rangle, \quad (26)$$

where n_F and n_N are the number densities of F and N in the detector and $\langle\sigma_{\text{capt}}v\rangle$ is the thermally averaged capture cross section times the relative velocity

$$\langle\sigma_{\text{capt}}v\rangle = \int\sigma_{\text{capt}}vP(\vec{v_F}^{\text{lab}})P(\vec{v_N}^{\text{lab}})d^3v_F^{\text{lab}}d^3v_N^{\text{lab}}. \quad (27)$$

Passing to center-of-mass and relative velocities $\vec{v}_{\text{CM}}$ and $\vec{v}$, using (24)–(27), and performing the integration over the center-of-mass variables, we get

$$R = 8n_F n_N\frac{1}{(2\pi T)^{3/2}}\frac{1}{\mu^{1/2}}\int_0^\infty\sigma_{\text{capt}}(E)Ee^{-E/T}dE, \quad (28)$$

where $E = \frac{1}{2}\mu v^2$ is the total energy in the center-of-mass frame.

Considering the annual modulation scenario and requiring that the density of particles F in the detector is determined by the equilibrium between the incoming flux at the terrestrial surface and the down-drifting thermalized flux, driven by gravity, one can write down the number density n_F within the detector as a function modulated in time:

$$n_F = n_F^0 + n_F^m \cos(\omega(t - t_0)), \tag{29}$$

where $\omega = \frac{2\pi}{T_{\rm orb}}$ is the angular frequency of the orbital motion of the Earth around the Sun and $t_0 \simeq$ June 2 is the period of the year when the Earth and Sun orbital velocities are aligned. The constant part is given by

$$n_F^0 = \frac{n_0 n \langle \sigma_{\rm at} v \rangle}{4g} V_h \tag{30}$$

while the annual modulation of the concentration is characterized by the amplitude

$$n_F^m = \frac{n_0 n \langle \sigma_{\rm at} v \rangle}{4g} V_E \cos\gamma. \tag{31}$$

$V_h = 220 \times 10^5$ cm/s is the orbital velocity of the Sun around the galactic center, $V_E = 29.5 \times 10^5$ cm/s is the Earth orbital velocity around the sun, $\gamma \simeq 60°$ is the inclination angle of the Earth orbital plane with respect to the galactic plane, $n_0 = \frac{3\times10^{-4}}{S_3}$ cm^{-3} is the local density of the dark atoms, $n \simeq 5 \times 10^{22}$ cm^{-3} is the number density of atoms in the terrestrial crust, $g = 980$ cm/s^2 is the acceleration of gravity and $n\langle\sigma_{\rm at} v\rangle$ is the rate of elastic collisions between a thermalized dark atom FG and terrestrial atoms. $\sigma_{\rm at}$ is obtained by integrating the differential cross section (14) from Sec. IV B over all diffusion angles in the case of a silicon atom and v is the relative velocity between a dark atom and a terrestrial atom. Note that $\sigma_{\rm at}$ dominates over $\sigma_{\rm nucl}$ at low energies, so there is no need to consider $\sigma_{\rm tot}$ here.

Expression (29) may be inserted into (28) to get an annually modulated counting rate per unit volume of the detector,

$$R = R^0 + R^m \cos(\omega(t - t_0)). \tag{32}$$

In counts per day and per kilogram (cpd/kg) of detector, the constant and modulated parts of the signal will respectively be given by

$$\begin{aligned} R^0 &= C n_F^0 \int_0^\infty \sigma_{\rm capt}(E) E e^{-E/T} dE, \\ R^m &= C n_F^m \int_0^\infty \sigma_{\rm capt}(E) E e^{-E/T} dE \end{aligned} \tag{33}$$

with

$$C = 24.10^{10} \frac{Q t N_{Av}}{M_{\rm mol}} \frac{1}{(2\pi T)^{3/2}} \frac{1}{\mu^{1/2}},$$

where $Q = 1000$ g, $t = 86400$ s, $N_{Av} = 6.022 \times 10^{23}$ and $M_{\rm mol}$ is the molar mass of the active medium of the detector in g/mol.

VI. RESULTS

The presented model intends to reproduce the positive results of direct dark matter searches experiments, such as DAMA/LIBRA and CoGeNT, without contradicting the negative results of some others, such as XENON100 or CDMS-II/Ge.

The DAMA/LIBRA experiment observes an integrated modulation amplitude $\tilde{R}^m_{\rm DAMA} = (0.0464 \pm 0.0052)$ cpd/kg in the energy interval (2–6) keV [1], while the temporal analysis of CoGeNT has given $\tilde{R}^m_{\rm CoGeNT} = (1.66 \pm 0.38)$ cpd/kg in the interval (0.5–2.5) keV [21].

Here, in a first approximation and for simplicity, the signal is supposed to be made of one monochromatic line of energy $\Delta E_{\rm DAMA}$, $\Delta E_{\rm CoGeNT}$. It would be very interesting to reproduce the observed energy distributions of the rates by taking into account the possible transitions to the different s states, but this is postponed to another paper.

One first solves the Schrodinger equation independent on time with potential $V^N = V_C^N + V_M^N$ in cases of iodine (^{127}I component of DAMA/LIBRA detector), germanium (^{74}Ge component of CoGeNT detector) and xenon (^{132}Xe component of XENON100 detector) with the WKB approximation. This gives good estimates of the eigenvalues and eigenfunctions of the respective two-body bound state problems. The bound eigenfunctions are normalized numerically before computing the constant or modulated number density of F particles (30) or (31). The constant or modulated part of the event rate is finally computed for each nucleus from (33) with the expression (24) of the capture cross section, at the operating temperatures of the different detectors, i.e. $T = 300$, 73, and 173 K for DAMA/LIBRA, CoGeNT, and XENON100, respectively.

One set of parameters that reproduces the data well and the corresponding transitions energies (ΔE), lowest levels at $l = 1$ ($E^{l=1}$) and rates (R^0 and R^m) are given in Table I.

The energies of the signals and the event rates are well reproduced for the DAMA and CoGeNT experiments.

TABLE I. Best fit parameters and predicted transitions energies and event counting rates for DAMA/LIBRA, CoGeNT and XENON100 experiments.

	m_F (GeV)	m_S (MeV)	ϵ	η
Best fit	650	0.426	6.7×10^{-5}	2.2×10^{-7}
	ΔE (keV)	$E^{l=1}$ (keV)	R^0 (cpd/kg)	R^m (cpd/kg)
DAMA/LIBRA	3.8	−2.0	⋯	0.045
CoGeNT	1.4	−0.4	⋯	1.673
XENON100	4.1	−2.3	8.455×10^{-5}	⋯

The lowest levels at $l = 1$ give rise to E1 captures that emit photons at threshold (2 keV for DAMA) or below threshold (0.5 keV for CoGeNT) and only the photon emitted during the second E1 transition from a p state to an s state is observed, making the captures look like single-hit events. The low predicted rate for XENON100 corresponds, over the total exposure of the experiment [5], to $\simeq 0.6$ events. Therefore, no dark matter event should have occurred within the XENON100 detector, which is consistent with observations. Moreover, let us recall that a few events happening during the exposure would not be problematic since they would produce electron recoils and would be interpreted as backgrounds and ignored. Also, if we set $g' = g$, so that $\eta = \tilde{\eta}$, the best fit value of η is well below the limit (9) obtained from vector meson disintegrations.

Computing the penetration length (18) with the parameters of Table I, one finds that the dark atoms thermalize after $\simeq 40$ m, so that they reach the detectors at thermal energies, as required by the model and already announced in Sec. IV D.

In a cooled detector, the dark atoms also have to thermalize when they pass from the laboratory room to the active medium, i.e. at the edge of the detector or over a distance smaller than its size. One can roughly estimate the penetration in a detector with the same formula (18), by setting $E_0 = \frac{3}{2}T_{\text{room}}$ and $E_{\text{th}} = \frac{3}{2}T$, even if here the motions of the atoms in the thermalizer should be taken into account and the straight-line-path approximation is more questionable. This gives, for CoGeNT and XENON100, penetration lengths $\simeq 1$ Å, which is clearly much smaller than the size of the detectors and corresponds to thermalizations directly at the edges.

This model predicts an event rate consistent with zero in any cryogenic detector ($T \simeq 1$ mK), due to the Coulomb barrier of the nucleus-F potential that prevents particles with very small energies to be captured in the well. This is in agreement with the negative results of the cryogenic CDMS-II/Ge (germanium) experiment, in which thermalization when entering the detector is realized after $\simeq 1$ μm.

In the same manner, we predict no events in the cryogenic CDMS-II/Si (silicon) and CRESST-II detectors, in contradiction with the three events recently observed by the former and the signal of the latter. However, the penetration length in a cryogenic detector made of silicon as CDMS-II/Si is $\simeq 1$ mm,[1] i.e. 3 orders of magnitude larger than its equivalent in germanium. This is essentially due to the smaller electric charge of a silicon nucleus, giving a weaker stopping power. In this case, more collisions happen near the edge of the detector, while the dark atoms are still at room temperature and hence more likely to cross the Coulomb barrier. These peripheral collisions should therefore be studied in detail, together with the possibility that the interactions of the emitted photons could be misinterpreted as nuclear recoils, to explain the events of some cryogenic detectors.

In this analysis, attention has been paid to the iodine component of the DAMA detector, while it is constituted by a crystal of NaI, and hence also of sodium. Some part of the signal could come from this other component, but it turns out that the only bound state with ^{23}Na is very shallow (-61 eV) and is at $l = 0$. There is therefore no p state on which the capture can happen, and the signal of DAMA is due only to its iodine component. One can try to reproduce data directly with the sodium component, but in that case the levels obtained afterward with iodine are much too low (because the potential well is lower, as seen in Fig. 3) and give rise to a signal out of the detection interval of DAMA.

The fact that DAMA data are reproduced with the heavy component, iodine, and not with the light one, sodium, is in fact an advantage of the model, since in this situation, light isotopes do not have any bound states with dark atoms. The first element presenting an s bound state is oxygen ($Z = 8$) while the first one having at least one p bound state is phosphorus ($Z = 15$). Binding is therefore impossible for very light nuclei with $Z \leq 7$, preventing the formation of anomalous isotopes during big bang nucleosynthesis, while heavy isotopes cannot form on Earth with nuclei $Z \leq 14$, representing the majority of terrestrial elements.

VII. CONCLUSION

We have presented a model in which a fraction of the dark matter density (5% or less) is realized by two new species of fermions F and G, forming hydrogenoid atoms with standard atomic size through a dark $U(1)$ gauge interaction carried out by a dark massless photon. Dark scalar particles S are exchanged by the nuclei F because of a Yukawa coupling between F and S. A kinetic photon-dark photon mixing and a mass σ-S mixing, respectively characterized by small dimensionless mixing parameters ϵ and η, induce interactions between the dark sector and the ordinary one. The dark atoms interact elastically in terrestrial matter until they thermalize, in such a way that they reach underground detectors with thermal energies. There, they form bound states with nuclei by radiative capture, causing the emission of photons that create the observed signals. The model reproduces well the positive results from DAMA/LIBRA and CoGeNT, without contradicting the negative results from XENON100 with the following parameters: $m_F = 650$ GeV, $m_S = 0.426$ MeV, $\epsilon = 6.7 \times 10^{-5}$ and $\eta = 2.2 \times 10^{-7}$. It naturally prevents

[1]We also have calculated the initial interaction length x_0 of a dark matter particle at room temperature entering a cold detector, $x_0^{-1} = n_m \int_\Omega (\frac{d\sigma}{d\Omega})_{\text{tot}} d\Omega$, for each of the cases CoGeNT, XENON100, CDMS-II/Ge, and CDMS-II/Si. For all of them, $x_0 \simeq 10^{-2}$ Å, which is always smaller than the computed penetration lengths x from (18). This is a way to check that the continuous energy loss approximation is still valid for the thermalization in cold detectors.

any signal in a cryogenic detector ($T \sim 1$ mK), which is consistent with CDMS-II/Ge. Further studies have to be performed to explain the presence of a signal in CRESST-II, and possibly in CDMS-II/Si, especially by considering the collisions of the dark atoms at the edge of the detector, when they are still at room temperature while the detector is colder.

ACKNOWLEDGMENTS

I am grateful to my advisor, J. R. Cudell, for key reading suggestions and many discussions concerning this work. My thanks go to M. Khlopov for inspiring ideas and discussions and to M. Tytgat for useful comments. I thank the Belgian Fund F.R.S.-FNRS, which funds me as a Research Fellow.

[1] R. Bernabei *et al.* (DAMA/LIBRA Collaboration), Eur. Phys. J. C **67**, 39 (2010).
[2] C. Aalseth *et al.* (CoGeNT Collaboration), Phys. Rev. D **88**, 012002 (2013).
[3] G. Angloher, M. Bauer, I. Bavykina, A. Bento, C. Bucci *et al.*, Eur. Phys. J. C **72**, 1971 (2012).
[4] R. Agnese *et al.* (CDMS-II Collaboration), arXiv:1304.4279.
[5] E. Aprile *et al.* (XENON100 Collaboration), Phys. Rev. Lett. **109**, 181301 (2012).
[6] Z. Ahmed *et al.* (CDMS-II Collaboration), Phys. Rev. Lett. **106**, 131302 (2011).
[7] R. Foot, Phys. Rev. D **86**, 023524 (2012).
[8] J. M. Cline, Z. Liu, and W. Xue, Phys. Rev. D **85**, 101302 (2012).
[9] M. Y. Khlopov, A. G. Mayorov, and E. Y. Soldatov, Prespacetime J. **1**, 1403 (2010).
[10] M. Y. Khlopov, A. G. Mayorov, and E. Y. Soldatov, in *Proceedings to the 14th Workshop "What Comes Beyond the Standard Model"*, edited by N. Mankoc Borstnik, H. B. Nielsen, C. D. Froggatt, and D. Lukman (DMFA, Ljubljana, 2011), pp. 94–102.
[11] J. Cudell, M. Khlopov, and Q. Wallemacq, in *Proceedings to the 15th Workshop "What Comes Beyond the Standard Model"*, edited by N. Mankoc Borstnik, H. B. Nielsen, and D. Lukman (DMFA, Ljubljana, 2012), pp. 10–27.
[12] J. Miralda-Escudé, Astrophys. J. **564**, 60 (2002).
[13] J. Fan, A. Katz, L. Randall, and M. Reece, arXiv:1303.1521.
[14] C. Amsler *et al.* (Particle Data Group Collaboration), Phys. Lett. B **667**, 1 (2008).
[15] G. Erkol, R. Timmermans, and T. Rijken, Phys. Rev. C **72**, 035209 (2005).
[16] S. D. McDermott, H.-B. Yu, and K. M. Zurek, Phys. Rev. D **83**, 063509 (2011).
[17] R. Balest *et al.* (CLEO Collaboration), Phys. Rev. D **51**, 2053 (1995).
[18] B. Aubert *et al.* (*BABAR* Collaboration), arXiv:0808.0017.
[19] J. Insler *et al.* (CLEO Collaboration), Phys. Rev. D **81**, 091101 (2010).
[20] E. Segre, *Nuclei and Particles* (W.A. Benjamin, Inc., New York, 1977), 2nd ed.
[21] C. Aalseth, P. Barbeau, J. Colaresi, J. Collar, J. Diaz Leon *et al.*, Phys. Rev. Lett. **107**, 141301 (2011).